

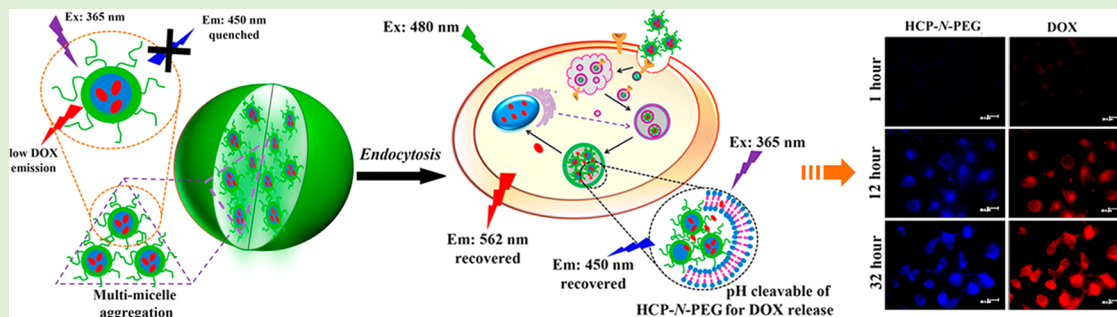
# Real-Time Monitoring of Anticancer Drug Release with Highly Fluorescent Star-Conjugated Copolymer as a Drug Carrier

Feng Qiu,<sup>†,‡</sup> Dali Wang,<sup>†</sup> Qi Zhu,<sup>\*,†</sup> Lijuan Zhu,<sup>†</sup> Gangsheng Tong,<sup>§</sup> Yunfeng Lu,<sup>\*,†,||</sup> Deyue Yan,<sup>†</sup> and Xinyuan Zhu<sup>\*,†</sup>

<sup>†</sup>School of Chemistry and Chemical Engineering, Shanghai Key Lab of Electrical Insulation and Thermal Aging, <sup>‡</sup>Department of Electronic Engineering, and <sup>§</sup>Instrumental Analysis Center, Shanghai Jiao Tong University, 800 Dongchuan Road, Shanghai 200240, People's Republic of China

<sup>||</sup>Department of Chemical and Biomolecular Engineering, University of California, Los Angeles, California 90095, United States

## Supporting Information



**ABSTRACT:** Chemotherapy is one of the major systemic treatments for cancer, in which the drug release kinetics is a key factor for drug delivery. In the present work, a versatile fluorescence-based real-time monitoring system for intracellular drug release has been developed. First, two kinds of star-conjugated copolymers with different connections (e.g., pH-responsive acylhydrazone and stable ether) between a hyperbranched conjugated polymer (HCP) core and many linear poly(ethylene glycol) (PEG) arms were synthesized. Owing to the amphiphilic three-dimensional architecture, the star-conjugated copolymers could self-assemble into multimicelle aggregates from unimolecular micelles with excellent emission performance in the aqueous medium. When doxorubicin (DOX) as a model drug was encapsulated into copolymer micelles, the emission of star-conjugated copolymer and DOX was quenched. In vitro biological studies revealed that fluorescent intensities of both star-conjugated copolymer and DOX were activated when the drug was released from copolymeric micelles, resulting in the enhanced cellular proliferation inhibition against cancer cells. Importantly, pH-responsive feature of the star-conjugated copolymer with acylhydrazone linkage exhibited accelerated DOX release at a mildly acidic environment, because of the fast breakage of acylhydrazone in endosome or lysosome of tumor cells. Such fluorescent star-conjugated copolymers may open up new perspectives to real-time study of drug release kinetics of polymeric drug delivery systems for cancer therapy.

## 1. INTRODUCTION

As one of the most promising methods for drug delivery in disease therapy, polymeric drug delivery systems (PDDSS) including polymeric micelles and polymer–drug conjugates exhibit several unique features,<sup>1–3</sup> such as improved water-solubility and bioavailability of hydrophobic drugs, prolonged *in vivo* drug circulation half-life, reduced systemic side effects, and preferential accumulation at the tumor sites by the enhanced permeability and retention (EPR) effect.<sup>4,5</sup> Therefore, PDDSS have attracted tremendous attention during the past decades.<sup>6–8</sup> To realize an efficient delivery of drugs, the drug release kinetics is a key factor, which represents how many and how fast the drugs release from the delivery carriers.<sup>9,10</sup> Up till now, several analytical techniques have been employed to monitor the drug release kinetics, including fluorescence detection,<sup>11–13</sup> magnetic resonance imaging,<sup>14,15</sup> ultrasound

imaging,<sup>16</sup> and electrochemistry measurement.<sup>17,18</sup> Among them, the fluorescence technique has been considered as a convenient and fundamental tool to quantitate the amount of released drugs in a complicated intracellular environment.

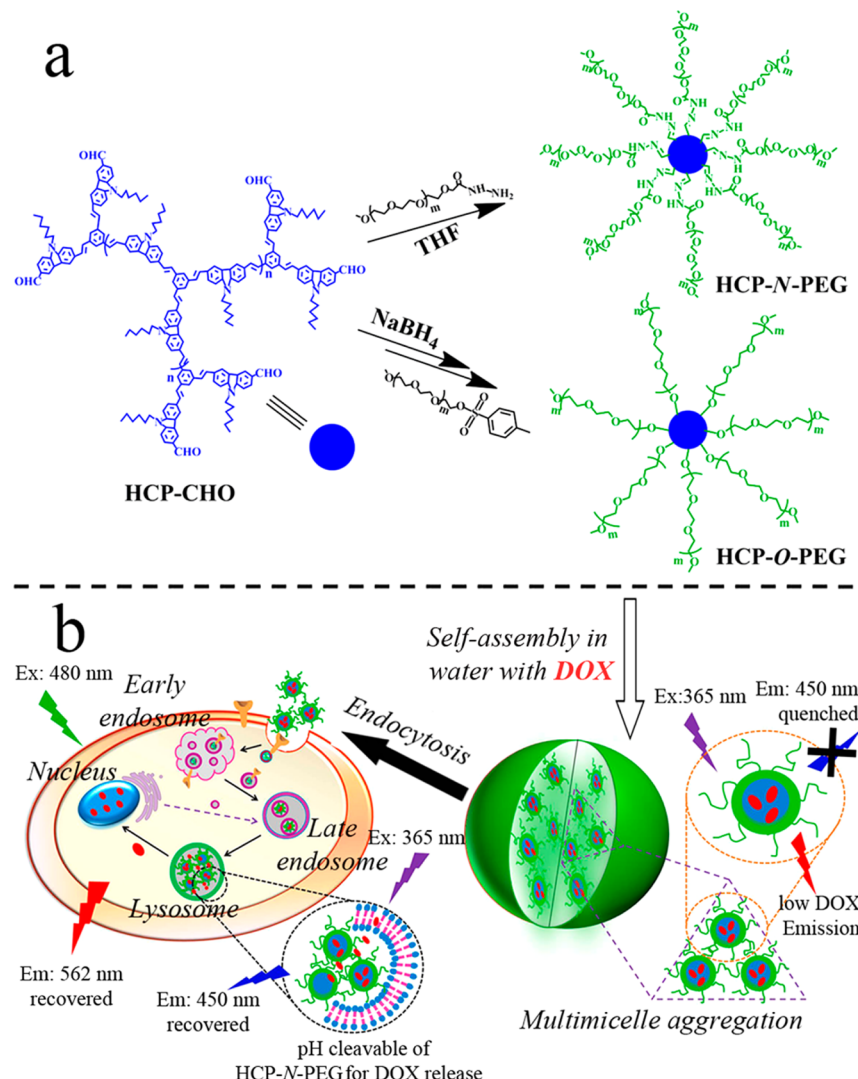
For fluorescence detection, the fluorescent probes such as small fluorophores and fluorescent proteins are usually introduced into the PDDSS.<sup>19,20</sup> Due to the specific activation between the drug and fluorescent probe, the drug release can be monitored through the “turn-on/turn-off” fluorescent signal.<sup>12</sup> However, these fluorescent probes usually suffer from the low photobleaching thresholds,<sup>21,22</sup> which limits the long-term and three-dimensional imaging. Different from small fluorophores,

**Received:** December 21, 2013

**Revised:** March 7, 2014

**Published:** March 7, 2014

**Scheme 1.** (a) Synthesis Route of HCP-N-PEG and HCP-O-PEG Star-conjugated Copolymers; (b) Self-Assembly of Star-Conjugated Copolymer and Their Endocytosis in the Tumor Cells



fluorescent conjugated polymers generally exhibit the bright optical properties, low photobleaching, and low toxicity to cells and living organisms that fulfills the requirements of real-time drug release monitoring.<sup>23–25</sup> Besides, the amplified fluorescent response of conjugated polymers shows superior sensitivity to those of small fluorophores.<sup>26</sup> Combining their high molecular weight, fluorescent conjugated polymers show the potential for real-time monitoring of drug release in tumor cells. Unfortunately, the emission performance of conjugated polymers is often deteriorated by  $\pi-\pi$  stacking of hydrophobic conjugated segments in an aqueous solution. Thus, design of conjugated polymers with high fluorescence for real-time monitoring of drug release from delivery systems is much desirable.

Very recently, we have noticed that the star-conjugated copolymers with a dendritic conjugated core and many linear arms show good fluorescent performance through self-assembling into multimicelle aggregates from unimolecular micelles without phase separation.<sup>27–29</sup> The three-dimensional dendritic architecture and self-assembly behavior of star-conjugated copolymers favor the encapsulation of hydrophobic drugs. Considering that most hydrophobic drugs have a

conjugated structure, it can be imagined that the encapsulation of hydrophobic drugs into the star-conjugated copolymers will result in the change of fluorescence. As long as the drugs release from the conjugated polymer carriers, the fluorescence of both drug and conjugated polymer will be recovered. Correspondingly, the drug release kinetics in different conditions can be readily tracked by detecting the fluorescence variation of both drug and conjugated polymer. In the present work, we constructed two kinds of star-conjugated copolymers containing the HCP core and many linear PEG arms: pH-responsive polymer (HCP-N-PEG) with acyldydrazone linkage and control polymer (HCP-O-PEG) with stable ether linkage (Scheme 1a). Benefiting from their amphiphilicity and special three-dimensional architecture, the star-conjugated copolymers self-assembled into micelles in an aqueous medium with excellent emission performance, which could be used as polymeric carriers for real-time monitoring of drug release in the tumor cells (Scheme 1b). The emission of polymeric micelles would be quenched when the hydrophobic drug DOX was encapsulated into the polymeric micelles. With the release of DOX from micelles, fluorescence of polymeric micelles and DOX were recovered. Due to the macropinocytosis of

polymeric micelles, the release kinetics discrepancy of DOX between HCP-N-PEG and HCP-O-PEG micelles could be directly distinguished.

## 2. EXPERIMENTAL SECTION

**2.1. Materials.** Hyperbranched conjugated polymer with aldehyde terminal group (HCP-CHO), hyperbranched conjugated polymer with hydroxyl terminal group (HCP-CH<sub>2</sub>OH), and star-conjugated copolymer (HCP-N-PEG) were synthesized according to the method described in our previous papers.<sup>29,30</sup> Sodium borohydride (NaBH<sub>4</sub>, C.P. grade, Shanghai Chemical Reagent Co.), hydrazine hydrate (85%, C.P. grade, Shanghai Chemical Reagent Co.), *p*-toluenesulfonyl chloride (TsCl, C.P. grade, Shanghai Chemical Reagent Co.), sodium hydride (NaH, 60%, Fluka), 3-(4,5-dimethyl-thiazol-2-yl)-2,5-diphenyl tetrazolium bromide (MTT, Sigma), doxorubicin hydrochloride (DOX-HCl, Beijing Huafeng United Technology Corporation), and poly(ethylene glycol) monomethyl ether (PEG, Fluka,  $M_n = 2000$ ) were used as received. Dulbecco's modified Eagle's medium (DMEM), fetal bovine serum (FBS), and phosphate buffered solution (PBS) were purchased from PAA Laboratories GmbH. Cell lysis solution was from Promega. Dialysis tube (MWCO, 3.5 kDa) was from Shanghai Lvniao Technology Corp. Clear polystyrene tissue culture treated 6-, 24-, and 96-well plates were obtained from Corning Costar. Tetrahydrofuran (THF) was refluxed over sodium wires and benzophenone until anhydride and then distilled to use immediately. *N,N*-Dimethyl formamide (DMF), chloroform (CHCl<sub>3</sub>), and dichloromethane (CH<sub>2</sub>Cl<sub>2</sub>) were refluxed with calcium hydride and distilled before use. The other chemical reagents were purchased from domestic suppliers and used as received.

**2.2. Preparation of Poly(ethylene glycol) Monomethyl Ether *p*-Toluene Toluenesulfonate (PEG-OTs).** PEG with hydroxyl end-group (PEG-OH, 20.0 g, 10 mmol) was dissolved in 200 mL of CH<sub>2</sub>Cl<sub>2</sub> and cooled to 0 °C. Then, *p*-toluene sulfonyl chloride (TsCl, 2.3 g, 12 mmol) and KOH powder (1.8 g, 32 mmol) were added, respectively. The mixture was heated to room temperature overnight. After the reaction was completed, the mixture was filtered, washed with water and CH<sub>2</sub>Cl<sub>2</sub>. The organic phase was dried with anhydrous magnesium sulfate, concentrated under reduced pressure and precipitated into cold diethyl ether twice and filtered to obtain a white solid. Yield: 96%. <sup>1</sup>H NMR (400 MHz, CDCl<sub>3</sub>, ppm, 20 °C): 7.78 (d, 2H, Ar), 7.33 (d, 2H, Ar), 4.12 (t, 2H, Ar-OCH<sub>2</sub>CH<sub>2</sub>O-), 3.54–3.63 (m, 174H, -OCH<sub>2</sub>CH<sub>2</sub>O-), 3.35 (s, 3H, -OCH<sub>3</sub>), 2.43 (s, 3H, Ar-CH<sub>3</sub>).

**2.3. Preparation of HCP-O-PEG.** In a three-neck flask, NaH was added and washed by anhydrous THF. Then, HCP-CH<sub>2</sub>OH and PEG-OTs were dissolved in THF and pumped into the flask. The mixture was heated to reflux at 90 °C for 3 days under nitrogen. After cooled to room temperature, the solution was washed with deionized water several times, dried with anhydrous magnesium sulfate. After filtering, the solution was concentrated and precipitated three times with anhydrous methanol. The yellow precipitate was obtained after drying under vacuum at 40 °C. Yield: 85%. <sup>1</sup>H NMR (400 MHz, CDCl<sub>3</sub>, ppm, 20 °C): 0.45–0.98 (br, CH<sub>3</sub>), 0.98–1.45 (br, CH<sub>2</sub>CH<sub>3</sub>), 1.45–2.50 (br, NCH<sub>2</sub>CH<sub>2</sub>), 3.37 (br, OCH<sub>3</sub>), 3.38–3.98 (m, CH<sub>2</sub>CH<sub>2</sub>O), 4.05–4.42 (br, NCH<sub>2</sub>), 4.50–4.90 (br, Ar-CH<sub>2</sub>OH), 6.25–8.85 (m, Ar-H). <sup>13</sup>C NMR (100 MHz, CDCl<sub>3</sub>, ppm, 20 °C): 14.21 (CH<sub>3</sub>), 22.66 (CH<sub>2</sub>CH<sub>3</sub>), 27.03 (CH<sub>2</sub>CH<sub>2</sub>), 29.11 (CH<sub>2</sub>CH<sub>2</sub>), 29.85 (CH<sub>2</sub>CH<sub>2</sub>), 31.67 (NCH<sub>2</sub>CH<sub>2</sub>), 43.50 (NCH<sub>2</sub>), 59.22, 61.81 (OCH<sub>3</sub>), 69.51–72.81 (OCH<sub>2</sub>CH<sub>2</sub>), 109.43 (Ar-C), 123.12 (Ar-C), 128.77 (Ar-C), 132.23–134.27 (Ar-C), 138.29–140.74 (Ar-C), 144.27 (Ar-C). IR (KBr, cm<sup>-1</sup>): 3427, 2887, 1626, 1467, 1386, 1355, 1343, 1280, 1242, 1147, 1110, 1060, 963, 843, 529.

**2.4. Characterization.** <sup>1</sup>H and <sup>13</sup>C NMR spectra were recorded on a Varian Mercury Plus 400 MHz spectrometer with deuterated chloroform (CDCl<sub>3</sub>) and deuterated dichloromethane (CD<sub>2</sub>Cl<sub>2</sub>) as solvents at 20 °C. Tetramethylsilane (TMS) was used as the internal reference. Fourier transformed infrared (FTIR) spectra were recorded on a Paragon 1000 instrument by KBr sample holder method. The number-average molecular weight ( $M_n$ ) and the polydispersity ( $M_w/M_n$ )

were determined by gel permeation chromatography/multiangle laser light scattering (GPC-MALLS). The gel permeation chromatography system consisted of a Waters degasser, a Waters 515 HPLC pump, a 717 automatic sample injector, a Wyatt Optilab DSP differential refractometer detector, and a Wyatt miniDAWN multi-angle laser light scattering detector. Three chromatographic columns (styragel HR3, HR4, and HRS) were used in series. THF was used as the mobile phase at a flow rate of 1 mL min<sup>-1</sup> at 30 °C. The refractive index increment  $d\eta/dc$  was determined with Wyatt Optilab DSP differential refractometer at 690 nm. Data analysis was performed with Astra software (Wyatt Technology). Thermogravimetric analysis (TGA) measurements were performed on a Perkin-Elmer TGA-7 thermogravimetric analyzer to investigate the thermal stability of all samples in nitrogen atmosphere from ambient temperature to 700 °C at a heating rate of 20 °C min<sup>-1</sup>. Transmission electron microscopy (TEM) studies were performed with a JEOL 2010 instrument at a voltage of 200 kV. Samples were prepared by drop-casting micelle solutions onto carbon-coated copper grids, and then air-drying at room temperature before measurement. Dynamic light scattering (DLS) measurements were performed with a Malvern Zetasizer Nano S apparatus (Malvern Instruments Ltd.) equipped with a 4.0 mW He-Ne laser operating at 633 nm. All samples were measured at room temperature and a scattering angle of 173°. UV-vis measurements were performed on the Thermo Evolution 300 UV/vis spectrometer in the range of 200–800 nm. Photoluminescence (PL) spectra were recorded on QC-4-CW spectrometer, made by Photon Technology International, Int. USA/CAN. PL quantum yield ( $\Phi$ ) was determined by using the 9,10-diphenylanthracene as standard.<sup>31</sup>

**2.5. Formation of Self-Assembled HCP-N-PEG and HCP-O-PEG Micelles.** Star-conjugated copolymer (40 mg) dissolved in THF (4 mL) was stirred uniformly before use. Under gentle stirring, deionized water was added dropwise into THF solution. Then the THF was removed by dialyzing against deionized water for 24 h (MWCO = 2000), during which the water was renewed every 4 h. The final concentration of HCP-N-PEG and HCP-O-PEG in the resultant solution was diluted with deionized water. All procedures were performed at room temperature.

**2.6. pH Degradation of HCP-N-PEG.** A total of 10 mL of self-assembled HCP-N-PEG aqueous solution (5 mg mL<sup>-1</sup>) was added to the acetate buffer (pH 5.0) solution. After stirring uniformly for 12 h, the aqueous solution was extracted with CH<sub>2</sub>Cl<sub>2</sub>, and the organic layer was concentrated under reduced pressure. The product was obtained after drying under vacuum at 40 °C. The degradation of HCP-N-PEG was confirmed by the <sup>1</sup>H NMR spectra with CDCl<sub>3</sub>.

**2.7. Preparation of DOX-Loaded HCP-N-PEG and HCP-O-PEG Micelles.** Briefly, DOX-HCl and an equal molar amount of triethylamine (TEA) were dissolved in dimethyl sulphoxide (DMSO) and added to a THF solution of star-conjugated copolymer at a theoretical drug loading content of 10 wt %. Then the mixture was added slowly to 5 mL of PBS (50 mM, pH 7.4). After being stirred for an additional 4 h, the solution was dialyzed against deionized water for 24 h (MWCO = 2000), during which the water was renewed every 4 h. For determination of drug loading content, the DOX-loaded micelle solution was lyophilized and then dissolved in DMF. The UV absorbance at 485 nm was measured to determine the DOX concentration. Drug loading content (DLC) and drug loading efficiency (DLE) were calculated according to the following formula:

$$\text{DLC(wt\%)} = (\text{weight of loaded drug}/\text{weight of polymer}) \times 100\%$$

$$\text{DLE(wt\%)} = (\text{weight of loaded drug}/\text{weight of drug in feed}) \times 100\%$$

**2.8. In Vitro Drug Release.** A total of 6 mL of DOX-loaded micelles was transferred to a dialysis bag (MWCO = 2000). It was immersed in 75 mL of phosphate buffer (pH 7.4) or acetate buffer (pH 5.0) solutions in a shaking water bath at 37 °C to acquire sink conditions. At predetermined time intervals, 2 mL of the external buffer was withdrawn and replenished with an equal volume of fresh medium. The amount of released DOX was analyzed with fluorescence

spectrophotometer with the excitation at 480 nm. The release experiments were conducted in triplicate, and the results were the average data.

**2.9. Cell Cultures.** NIH/3T3 normal cells (a mouse embryonic fibroblast cell line) and MCF-7 cells (a human breast adenocarcinoma cell line) were cultured in DMEM supplied with 10% FBS, and antibiotics (50 units  $\text{mL}^{-1}$  penicillin and 50 units  $\text{mL}^{-1}$  streptomycin) at 37 °C under a humidified atmosphere containing 5%  $\text{CO}_2$ .

**2.10. In Vitro Cytotoxicity Assay.** The relative cytotoxicity of HCP-N-PEG and HCP-O-PEG micelles against NIH/3T3 cells was estimated by MTT viability assay. In the MTT assay, NIH/3T3 cells were seeded into 96-well plates with a density of  $1 \times 10^4$  cells per well in 200  $\mu\text{L}$  of medium. After 24 h of incubation, the culture medium was removed and replaced with 200  $\mu\text{L}$  of a medium containing serial dilutions of micelles. The cells were grown for another 48 h. Then, 20  $\mu\text{L}$  of 5 mg  $\text{mL}^{-1}$  MTT assays stock solution in PBS was added to each well. After incubating the cells for 4 h, the medium containing unreacted dye was removed carefully. The obtained blue formazan crystals were dissolved in 200  $\mu\text{L}$  per well DMSO and the absorbance was measured in a BioTek Elx800 at a wavelength of 490 nm.

**2.11. Flow Cytometry.** Flow cytometry was used to provide statistics on the uptake of DOX-loaded polymeric micelles into MCF-7 cells. MCF-7 cells ( $5.0 \times 10^5$  cells per well) were seeded in six-well culture plates and grown overnight. Then, the DOX-loaded polymeric micelles dissolved in DMEM culture medium with the DOX-loaded polymeric micelles at a final DOX concentration of 20  $\mu\text{g mL}^{-1}$  were added to different wells, and the cells were incubated at 37 °C for 15, 30, and 180 min. After the incubation, samples were prepared for flow cytometry analysis by removing the cell growth medium, rinsing with cold PBS, and treating with trypsin. Data for  $1.0 \times 10^4$  gated events were collected and analysis was performed by means of a BD Calibur flow cytometer and CELLQuest software.

**2.12. Assessment of Intracellular Fluorimetric Activation of DOX-Loaded Polymeric Micelles.** MCF-7 cells were seeded in 96-well plates at  $1 \times 10^4$  cells per well in 200  $\mu\text{L}$  of complete DMEM and cultured for 24 h, followed by removing culture medium and 200  $\mu\text{L}$  of a medium with DOX-loaded polymeric micelles at a final DOX concentration of 5  $\mu\text{g mL}^{-1}$ . The cells were incubated at 37 °C for predetermined intervals. Subsequently, the cells were washed with PBS three times, and the well was vibrated after cell lysate added for 1 h. The fluorescence intensities of polymeric micelles and DOX were recorded by fluorescence spectrophotometer with the excitation at 365 and 480 nm, respectively.

**2.13. Intracellular Monitoring of Drug Release for DOX-Loaded Polymeric Micelles.** MCF-7 cells ( $1.0 \times 10^4$  cells per well) were seeded on coverslips in a 24-well tissue culture plate. After 24 h of culture, 600  $\mu\text{L}$  of a medium with DOX-loaded polymeric micelles at a final DOX concentration of 5  $\mu\text{g mL}^{-1}$ , and the cells were incubated at 37 °C at predetermined time intervals. After being washed with PBS, the cells were fixed with 4% formaldehyde for 30 min at room temperature, and the slides were rinsed with PBS three times. Finally, the slides were mounted and observed with a Leica DMI6000B inverted fluorescence microscope. The excitation wavelengths of polymeric micelles and DOX are 360/40 nm and 546/12 nm, respectively.

**2.14. Assessment of Intracellular Cytotoxicity Activation of DOX-Loaded Polymeric Micelles.** MCF-7 cells were seeded in 96-well plates at  $1 \times 10^4$  cells per well in 200  $\mu\text{L}$  of complete DMEM and cultured for 24 h, followed by removing culture medium and adding 200  $\mu\text{L}$  of a medium with DOX-loaded polymeric micelles at a final DOX concentration of 5  $\mu\text{g mL}^{-1}$ . The cells were incubated at 37 °C for predetermined intervals. Subsequently, 20  $\mu\text{L}$  of 5 mg  $\text{mL}^{-1}$  MTT assay stock solution in PBS was added to wells. After incubating the cells for 4 h, the medium containing unreacted dye was removed carefully. The obtained blue formazan crystals were dissolved in 200  $\mu\text{L}$  per well DMSO and the absorbance was measured in a BioTek Elx800 at a wavelength of 490 nm.

**2.15. Endocytosis Pathway Study.** Intracellular localization of polymeric micelles was investigated in MCF-7 cells using immune labeling of organelles. MCF-7 cells ( $1.0 \times 10^4$  cells per well) were

seeded on coverslips in a 24-well tissue culture plate. After 24 h of culture, cells were incubated with 600  $\mu\text{L}$  of a medium with polymeric micelles at final concentration of 0.5 mg  $\text{mL}^{-1}$  at 37 °C, then washed twice with PBS, and fixed for 10 min at room temperature with 200  $\text{mL}$  of 4% PFA. For immune labeling, cells were permeabilized for 10 min with 3% Triton X-100 (in PBS), saturated with PBS containing 0.1% saponin and 2% FCS, then incubated with specific primary anti-Rab 5 antibodies against early endosomes. After 2 h of incubation, cells were washed and incubated for 2 h in darkness with secondary antibodies coupled with Alexa Fluor488 diluted to 1/400. Finally, the slides were mounted and observed with a Leica DMI6000B inverted fluorescence microscope.

### 3. RESULTS AND DISCUSSION

**3.1. Preparation and Characterization of Star-Conjugated Copolymers.** The synthesis routes of two star-conjugated copolymers containing HCP core and linear PEG arms are described in Scheme 1. First, the HCP core with aldehyde terminal group (HCP-CHO) was synthesized through  $\text{A}_2 + \text{B}_3$ -type Wittig coupling reaction.<sup>30</sup> According to the  $^1\text{H}$  NMR analysis, the degree of branching (DB) of the HCP core was calculated to be about 0.62 (see Figure S1). The aldehyde group of HCP-CHO was then reacted with PEG-acetylhydrazine terminals to give a star-conjugated copolymer with pH-sensitive acylhydrazone connection, named as HCP-N-PEG. As shown in Figure S2d, the peaks at  $\delta = 9.7$  and 10.2 ppm are attributed to protons of acylhydrazone bond. The PEG signal at  $\delta = 3.65$  ppm is observed, confirming the successful grafting of PEG arms onto HCP-CHO core. As a control, the HCP with hydroxyl group (HCP- $\text{CH}_2\text{OH}$ ) was prepared by reduction of HCP-CHO with sodium borohydride (see Figure S2),<sup>29</sup> and then the star-conjugated copolymer with ether connection (HCP-O-PEG) was obtained through the reaction between PEG-OTs and HCP- $\text{CH}_2\text{OH}$ . In Figure S2c, both proton peaks of HCP and PEG are also observed. Since the mole feed ratio of core and arm in the reaction is almost the same, the obtained grafting ratios of HCP-N-PEG and HCP-O-PEG are very close, which are 0.95 and 0.92, respectively. The detailed characterizations of HCP core and star-conjugated copolymers are listed in the Supporting Information (see Figures S1–S5).

Both HCP core and star-conjugated copolymers could be well dissolved in a wide range of organic solvents, such as THF,  $\text{CH}_2\text{Cl}_2$ , chloroform ( $\text{CHCl}_3$ ), and toluene. As shown in Figure 1, the optical properties of HCP-N-PEG and HCP-O-PEG are very similar to those of HCP-CHO core in THF. The UV-vis absorption peaks of HCP-CHO at 256 and 312 nm are attributed to  $\pi-\pi^*$  excitations of 3,6-carbazole unit, while the shoulder peak at 351 nm is related to both the phenylene-ethylene and carbazole-aldehyde moieties.<sup>29</sup> When the polymer is excited at 365 nm, the emission appears at 415 and 437 nm. After grafting with PEG, both absorption spectra and fluorescence spectra of HCP-N-PEG and HCP-O-PEG show little red- or blue-shift, indicating that the flexible PEG arms have no profound impact on the conformation of HCP core in THF solvent (Table 1 and Figure 1). However, the grafting of PEG arms results in a minor decrease in the fluorescent quantum yield from 33.4% to 29.3 and 22.5% for HCP-N-PEG and HCP-O-PEG, respectively. The lower fluorescent efficiency results from the “insulating” properties of PEG arms to decrease UV-vis absorption of HCP core.<sup>32</sup>

**3.2. Formation and Characterization of Polymeric Micelles.** Due to their amphiphilic structures, these star-conjugated copolymers could self-assemble into micelles in an aqueous medium. Figure 1 and Table 1 give their optical

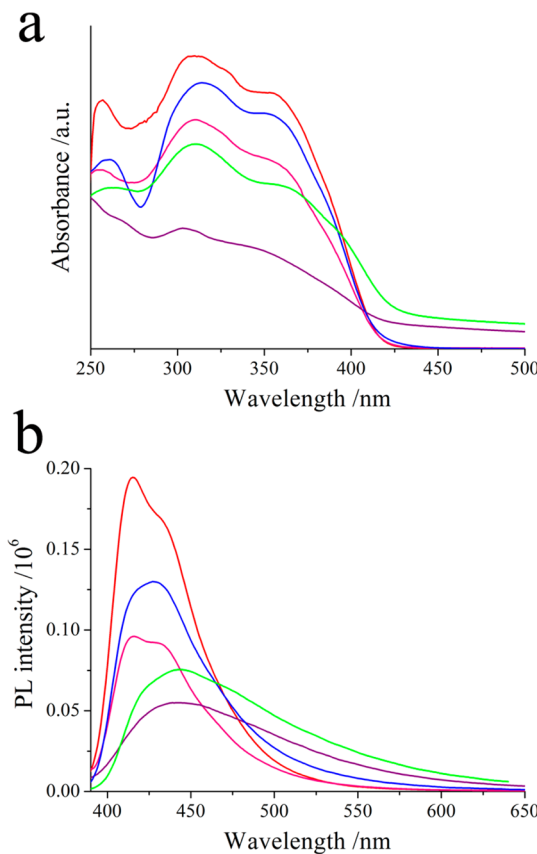


**Figure 1.** Absorption (a) and fluorescent (b) spectra of HCP-CHO (red), HCP-N-PEG (blue and green) and HCP-O-PEG (pink and purple) in THF and H<sub>2</sub>O, respectively.

**Table 1. Spectral Properties of HCP-CHO, HCP-N-PEG, and HCP-O-PEG**

polymer	THF			H <sub>2</sub> O		
	$\lambda_{\text{abs}}$ (nm)	$\lambda_{\text{em}}$ (nm)	$\Phi^a$ (%)	$\lambda_{\text{abs}}$ (nm)	$\lambda_{\text{em}}$ (nm)	$\Phi^a$ (%)
HCP-CHO	253, 305, 351	415, 432	33.4			
HCP-O-PEG	255, 310, 351	415, 432	22.5	267, 310, 362	444	3.3
HCP-N-PEG	260, 313, 355	416, 433	29.3	261, 310, 366	442	2.6

<sup>a</sup>Φ, PL quantum yield; 9,10-diphenylanthracene was used as standard.

properties. Compared with those THF solution, both absorption and fluorescent spectra of HCP-N-PEG and HCP-O-PEG in the aqueous solution become red-shift. Meanwhile, the fluorescent quantum yields of HCP-N-PEG and HCP-O-PEG decrease to 3.3 and 2.6%, respectively. This red-shift in fluorescent spectra indicates the intra- and intermolecular interactions of collapsed HCP core.<sup>28</sup> Due to the strong intermolecular interaction, the aggregation of hyperbranched poly(phenyleneethylene carbazole) usually results in the appearance of a new fluorescent peak at 475 nm. The disappearance of this peak in the PL spectra of HCP-N-PEG and HCP-O-PEG aqueous solution demonstrates that the severely intermolecular aggregation of HCP core is prevented by long PEG arms. These unique optical properties of HCP-N-PEG and HCP-O-PEG are realized through a “multimicelle aggregates” (MMA) mechanism of the star copolymers.<sup>28,33</sup>

The star-conjugated copolymer forms the unimolecular micelle first and then self-assembles into large micelles without phase separation. Thus, the collapsed HCP core shows good fluorescent intensity when well wrapped in the interior of unimolecular micelles by PEG arm. The self-assembled behaviors of HCP-N-PEG and HCP-O-PEG in the aqueous medium were determined by DLS and TEM measurements. As an example of HCP-N-PEG, the DLS curves in Figure S6a give a bimodal distribution. The small one at about 6 nm is related to the unimolecular micelles of star-conjugated copolymer; while the large one of around 65 nm comes from the self-assembled multimicelle aggregates. The TEM images in Figure S6b also reveal the coexistence of two dimensions of star copolymer nanoparticles in the aqueous medium, further confirming the MMA self-assembly mechanism of HCP-N-PEG. For HCP-O-PEG, similar results were observed (see Figures S6c and S6d). These results demonstrate that the different connection between the HCP core and PEG arms has no influence on their self-assembled behavior of star-conjugated copolymer with a similar grafting ratio of PEG.

The *in vitro* cytotoxicity of star-conjugated copolymer micelles was evaluated by MTT assay using NIH/3T3 normal cells. Figure 2 presents the cell viabilities after 48 h incubation

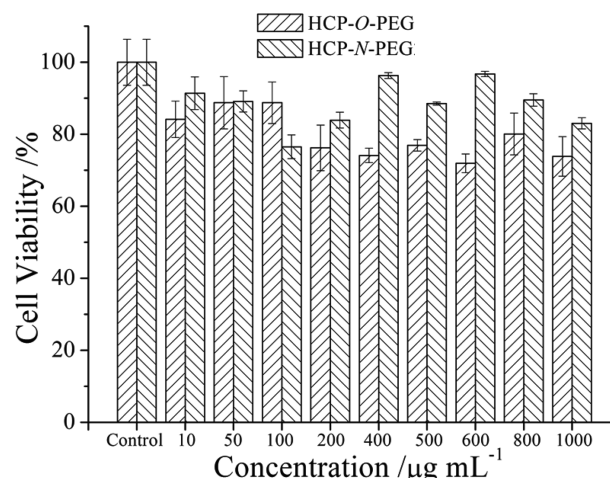


**Figure 2.** Cell viability of NIH/3T3 cells against HCP-N-PEG and HCP-O-PEG micelles after cultured for 48 h with different micelle concentrations.

with HCP-N-PEG and HCP-O-PEG micelles, respectively. Up to a concentration of 1 mg mL<sup>-1</sup>, cell viabilities are still above 80% compared to those of untreated cells. These results demonstrate that star-conjugated copolymers modified with biocompatible PEG show low cytotoxicity against NIH/3T3 normal cells. Therefore, both HCP-N-PEG and HCP-O-PEG micelles could be used as carriers for drug delivery.

**3.3. Preparation and Characterization of DOX-Loaded Polymeric Micelles.** To assess the potential application of star-conjugated copolymer micelles for real-time monitoring of drug release, DOX was used as a drug model to evaluate the drug loading and release properties. As a hydrophobic drug, DOX could be well encapsulated into the hydrophobic inner cores of star copolymeric micelles driven by the hydrophobic interactions between the drug and the hydrophobic segments of conjugated polymer. The theoretical DLC was set at 10%, the final DLC content of HCP-N-PEG was found to be 6.2% with DLE of 62.3%, and that of HCP-O-PEG was 5.6% with DLE of

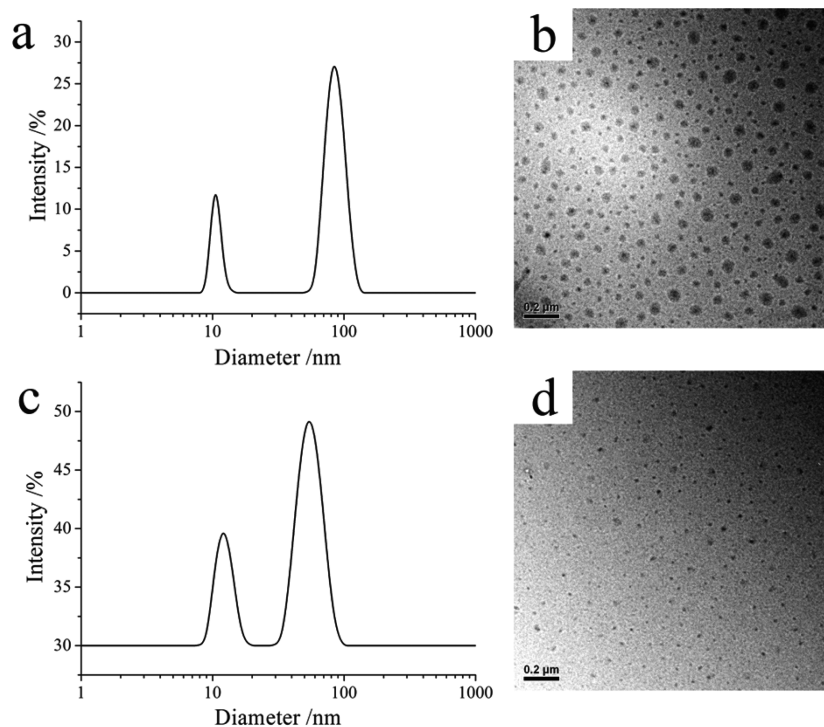


**Figure 3.** DLS plots and TEM photos of DOX-loaded HCP-O-PEG (a, b) and HCP-N-PEG (c, d) micelles; the scale bar represents 200 nm for b and d.

56.2%. The average sizes of DOX-loaded star copolymeric micelles were determined by DLS and TEM measurements. Both DOX-loaded HCP-N-PEG and HCP-O-PEG micelles show the bimodal distribution size (see Figure 3). The smaller one is about 12 nm, while the larger one is around 60–90 nm. The sizes of DOX-loaded star-conjugated copolymer micelles increase slightly compared with those of pure polymeric micelles. The increase of micelle sizes might result from the increase of hydrophobic core when DOX is encapsulated into star copolymer, which is in agreement with the thermodynamic aggregation of block copolymers.<sup>34</sup>

Importantly, the fluorescence of star-conjugated copolymer was quenched greatly upon encapsulation of DOX to polymeric micelles. As shown in Figure 4a, the emission intensity of the DOX-loaded HCP-O-PEG micelles at 450 nm decreases greatly with the excitation at 365 nm, compared with that of pure HCP-O-PEG micelles. The emission of HCP-O-PEG is quenched by the interaction between HCP core and DOX. Generally, free DOX shows a broad UV/vis absorption peak in the range of 400–600 nm, and the emission of DOX appears at 565 and 595 nm with the excitation at 480 nm (see Figure 4b). The UV/vis absorption spectrum of DOX overlaps well with the fluorescent spectrum of HCP-O-PEG, which leads to an efficient Förster resonance energy transfer (FRET) between HCP and DOX.<sup>35</sup> Thus, the fluorescent spectrum of DOX-loaded HCP-O-PEG micelles exhibits in the range of 550–600 nm, attributing to the emission of acceptor DOX. The energy transfer efficiency is inversely proportional to the distance between the donor HCP and the quencher DOX.<sup>36,37</sup> Therefore, it is understandable that mixing free DOX with polymeric micelles leads to significant fluorescence quenching of HCP-O-PEG. Collectively, these results demonstrate that fluorescence change of star-conjugated copolymer micelles could be used as the probes for real-time monitoring of the drug release in living tumor cells.

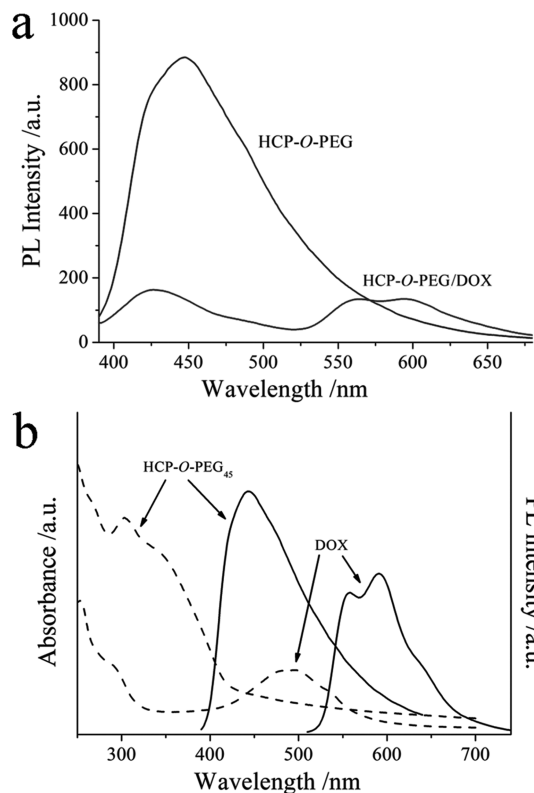


**Figure 4.** (a) Fluorescent spectra of HCP-O-PEG micelles and DOX-loaded HCP-O-PEG micelles at 1 mg mL<sup>-1</sup> concentration of the aqueous solution; (b) Normalized absorption (dashed) and fluorescent (solid) spectra of HCP-O-PEG micelles and DOX in the aqueous medium.

### 3.4. pH-Responsive Release of DOX from Polymeric Micelles.

As discussed above, the quenched fluorescence of

star-conjugated copolymer recovers once DOX releases from the polymeric micelles. To demonstrate this, we incubated DOX-loaded HCP-O-PEG in acetate buffer at pH 5.0 and measured the fluorescence spectra at different time intervals. As shown in Figure 5a, the fluorescence intensity of HCP-O-PEG

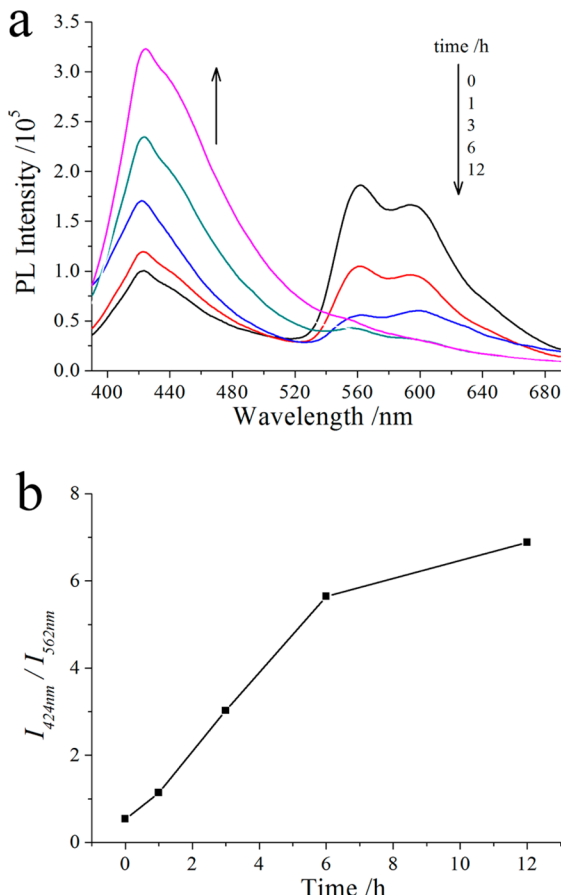


**Figure 5.** Fluorescent spectra of DOX-loaded HCP-O-PEG micelles as a function of dialysis time at 37 °C under pH 5.0. The final concentration was 1 mg mL<sup>-1</sup> (a); Plot of  $I_{424\text{nm}}/I_{562\text{nm}}$  vs dialysis time for DOX-loaded HCP-O-PEG micelles (b); Excitation wavelength was 365 nm.

( $I_{424\text{nm}}$ ) gradually recovers with increasing dialysis time. In the meantime, the emission of DOX ( $I_{562\text{nm}}$ ) decreases, which indicates that DOX releases out of polymeric micelles to avoid the quenching of HCP core. The plot of  $I_{424\text{nm}}/I_{562\text{nm}}$  as a function of dialysis time in Figure 5b shows that the recovery of HCP-O-PEG fluorescence intensity increases with the dialysis time.

To quantitatively determine DOX release from the polymeric micelles, DOX-loaded HCP-N-PEG and HCP-O-PEG micelles were suspended in either PBS at pH 7.4 or acetate buffer at pH 5.0 in a dialysis membrane tubing at 37 °C, which is used to simulate different intracellular environments: the pH 7.4 refers to the cytoplasm environment; while the pH 5.0 refers to the lysosome environment. The amount of released DOX at predetermined time intervals was measured by fluorescence measurement. As illustrated in Figure 6, the release profiles of DOX show a fast release from polymeric micelles in the first 12 h and then sustain a slow release over a prolonged time. For the HCP-O-PEG with ether connection, the cumulative release of DOX is lower than 30% of the DOX released in 160 h at pH

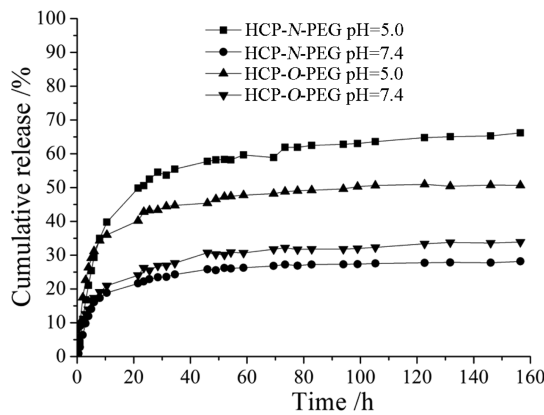


**Figure 6.** Cumulative release curves of DOX from DOX-loaded HCP-O-PEG and HCP-N-PEG micelles under different pH values (7.4 and 5.0) at 37 °C.

7.4; while at pH 5.0, the release ratio of DOX increases about 45% of the DOX released within 50 h. For the pH degradable HCP-N-PEG, the cumulative release of DOX from HCP-N-PEG micelles is still lower than 30% at pH 7.4 after 160 h. However, the cumulative release of DOX in HCP-N-PEG at pH 5.0 increases to 65%, which is much higher than that of HCP-O-PEG. In the neutral environment, the release of DOX from DOX-loaded HCP-O-PEG or HCP-N-PEG is caused mainly by concentration gradient between polymeric micelles and PBS solution. However, in an acid environment, DOX becomes hydrophilic, which promotes the cumulative release of DOX. It has been well realized that acylhydrazone bond is stable under neutral and basic conditions but will be hydrolyzed with the trigger of acid (pH < 5.5).<sup>38</sup> Thus, the cumulative release of DOX from DOX-loaded HCP-N-PEG micelles is similar to that of HCP-O-PEG in pH 7.4, but is much faster in pH 5.0. It demonstrates that the hydrolysis of acylhydrazone connection between HCP and PEG would accelerate the drug release from micelles. The pH-induced degradation of acylhydrazone connection in HCP-N-PEG is confirmed by <sup>1</sup>H NMR study (see Figure S7).

### 3.5. Accumulation and Retention of DOX in Cancer Cells.

Prior to using the DOX-loaded polymeric micelles for cellular internalization, we identified the cellular uptake of these micelles with DOX concentration of 20 µg mL<sup>-1</sup> by MCF-7 cells. The flow cytometry results show that relative geometrical mean fluorescence intensities of DOX after 15 min incubation with DOX-loaded HCP-O-PEG and HCP-N-PEG are much higher than that of nonpretreated cells (see Figure S8). These prominent fluorescence signals are associated with the attachment of DOX-loaded polymeric micelles onto MCF-7 cells.

To investigate the fluorescence change of DOX-loaded polymeric micelles in tumor cells, we incubated DOX-loaded polymeric micelles with MCF-7 cells over extended periods of time (0–12 h). The fluorescence spectra were determined by using fluorescence spectrophotometer after lysis of cells. Figure 7a shows a fast fluorescence activation of DOX-loaded polymeric micelles with the excitation at 365 nm during the first 2 h of incubation. This observation is caused by the rapid cellular uptake of polymeric micelles into MCF-7 cells, which is consistent with that of flow cytometry analysis. With the increase of incubation time, the emission intensity at 424 nm of cell-associated DOX-loaded polymeric micelles increases under

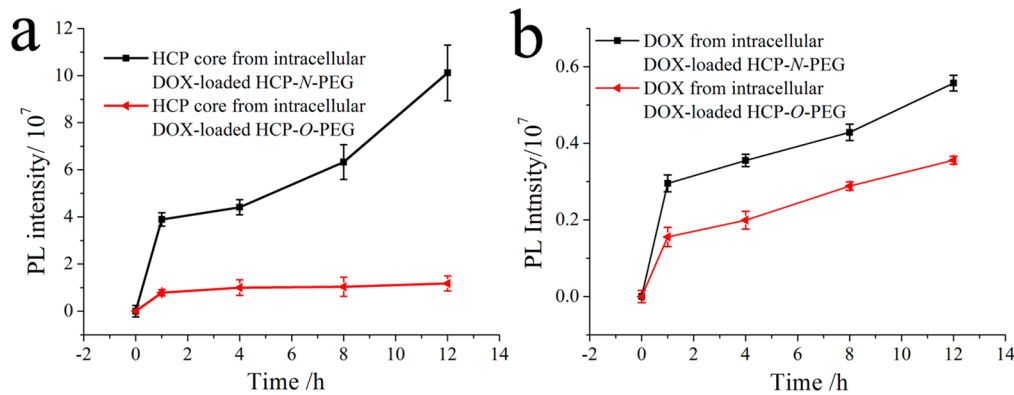


**Figure 7.** Time-dependent intracellular fluorescence emissions of HCP core under excitation at 365 nm (a) and DOX under excitation at 480 nm (b) from DOX-loaded HCP-N-PEG and HCP-O-PEG micelles in MCF-7 cells, respectively.

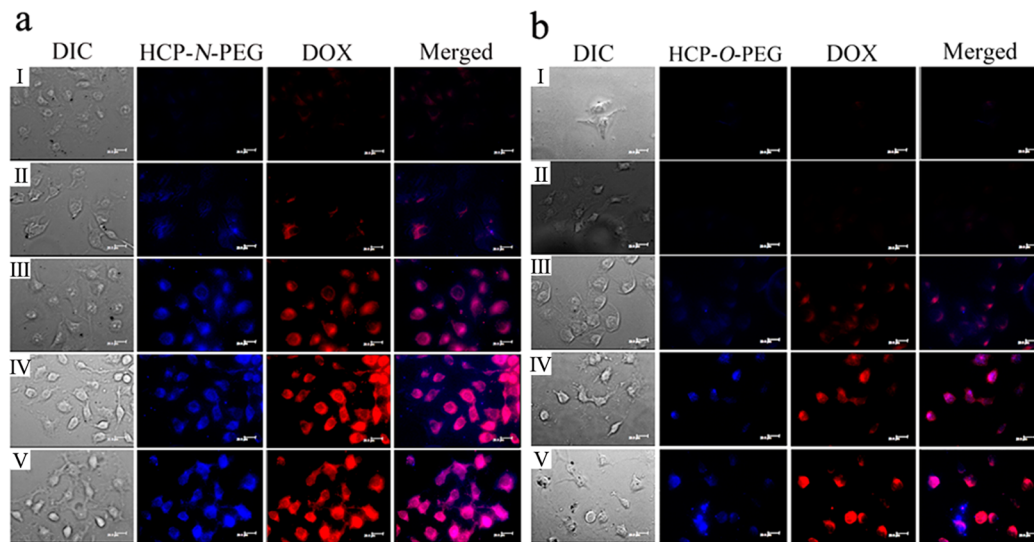


**Figure 8.** Time-dependent fluorescence microscope images of MCF-7 cells incubated with DOX-loaded HCP-N-PEG (a) and HCP-O-PEG (b) micelles; the incubation time was 1 (I), 4 (II), 12 (III), 20 (IV), and 32 h (V), respectively. The scale bar represents 20  $\mu$ m.

the excitation at 365 nm. This recovered fluorescence of star-conjugated polymers demonstrates the release of DOX from polymeric micelles in the tumor cells. Meanwhile, the fluorescence intensity of DOX also increases as expected with the increase of incubation time under the excitation at 480 nm (see Figure 7b). We also find that the DOX-loaded HCP-N-PEG micelles show a higher cell-associated fluorescence in tumor cells than that of DOX-loaded HCP-O-PEG micelles. A similar result also happens for the fluorescence of DOX. These findings confirm that pH-responsive degradation of HCP-N-PEG micelles promotes the release of DOX from polymeric micelles. These results also suggest that the entry mechanism of polymeric micelles into MCF-7 cells is macropinocytosis.<sup>39</sup> Therefore, the pH-responsive HCP-N-PEG micelles are degraded in the acidic endosome or lysosome to enhance the DOX release. To confirm the pH-degradation of HCP-N-PEG in the MCF-7 cells, intracellular trafficking of the internalized HCP-N-PEG micelles was investigated via colocalization of test particles and intracellular organelles (see Figure S9). The result shows that colocalization of HCP-N-PEG (blue) with the early endosomes (EEA1, green) is confirmed by the observed cyan color, due to an overlap of blue and green colors. Because the early endosomes mature into the late endosomes/lysosomes at longer incubation time, the above-mentioned observation

demonstrates that HCP-N-PEG micelles would be degraded to release DOX at an increased acidic environment from endosomes to lysosomes.<sup>39</sup>

It is important to demonstrate if we can correlate the fluorescence change of DOX-loaded polymeric micelles with the corresponding drug release and their consequent therapeutic efficacy.<sup>40–43</sup> To prove this, we treated MCF-7 cells with the addition of DOX-loaded HCP-N-PEG and HCP-O-PEG micelles, respectively. The cell-associated fluorescence changes with different incubation time were monitored by fluorescence microscope. As shown in Figure 8, the fluorescence intensities of star-conjugated copolymer and DOX are recovered with the increase of incubation time. Since the large size of polymeric micelles, these HCP-N-PEG micelles reside mainly in the cytoplasm of the cells.<sup>28</sup> In the meantime, the red fluorescence of DOX is mostly observed in the cytoplasm of cells before 12 h of incubation time. These results indicate that DOX-loaded polymeric micelles are taken up by the cells through a nonspecific endocytosis mechanism and the DOX is released in endocytic compartments. It is well-known that the free DOX is easy to accumulate in the nucleus.<sup>44,45</sup> Correspondingly, the red fluorescence from DOX diffuses from the cytoplasm to the whole cell when the incubation time is over 24 h. Compare with those of DOX-

loaded HCP-N-PEG micelles, DOX-loaded HCP-O-PEG micelles could also be internalized by MCF-7 cells, and fluorescence intensities of both star-conjugated copolymer and DOX are recovered with the increase of incubation time (see Figure 8b). The fluorescence of HCP-N-PEG micelles and DOX is observed after 4 h of incubation time, however, the release rate of DOX from HCP-O-PEG micelles is much slower, and the fluorescence of HCP-O-PEG micelles and DOX is detected after 12 h.

The cytotoxicity of DOX to the tumor cells is highly associated with the release of DOX from polymeric micelles.<sup>40</sup> Thus, the time-dependent cell viability of MCF-7 cells (2500 cells/well) was determined by MTT assay. The results in Figure 9 show a time-dependent decrease in the number of

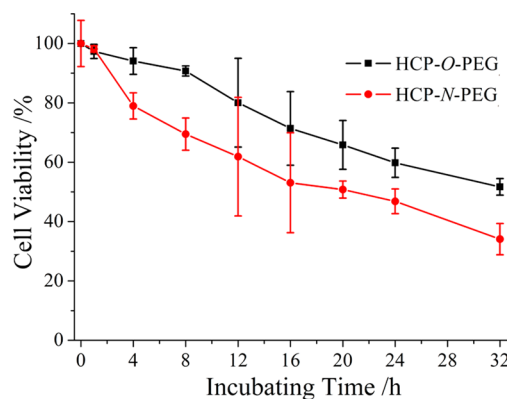


**Figure 9.** Cell viability of MCF-7 cells against DOX-loaded HCP-O-PEG and HCP-N-PEG micelles after incubation for 1, 4, 12, 20, and 32 h, respectively.

viable cells upon treatment with DOX-loaded polymeric micelles ( $1.2 \mu\text{M}$ ). As a control, only 50% cells are caused to death within 32 h for the more stable HCP-O-PEG micelles as drug carrier. However, the cell viability decreases greatly with the incubation of pH-responsive DOX-loaded HCP-N-PEG micelles, and more than 65% of cells are dead after 32 h. Owing to the low cytotoxicity of polymeric micelles, the death of tumor cells is caused by the released DOX from micelles. Compared to HCP-O-PEG micelles, the pH-responsive HCP-N-PEG micelles with quick drug release would trigger faster cell death, further confirming the same results found in fluorescence microscope. Thus, the drug release from polymeric micelles can be followed through the fluorescence changes of star-conjugated copolymer and DOX. The different releasing behavior of DOX between the pH-degradable HCP-N-PEG micelles and control HCP-O-PEG polymeric micelles could be directly observed by using star-conjugated copolymer with a hyperbranched conjugated copolymer core as drug carriers.

#### 4. CONCLUSIONS

In summary, we reported a novel fluorescence polymeric system as the drug carrier for real-time monitoring of intracellular drug release in the tumor cells. The star-conjugated copolymers with a HCP core and many linear PEG arms were synthesized. The structures and properties of two star-conjugated copolymers with pH-responsive acylhydrazone linkage (HCP-N-PEG) and control ether linkage (HCP-O-PEG) were characterized by  $^1\text{H}$  NMR, FTIR, UV-vis, and PL spectra. Owing to three-dimensional architecture, star-conjugated copolymers could self-assemble into polymeric micelles

with excellent fluorescence performance in the aqueous medium through multimicelle aggregate mechanism. When the DOX was encapsulated into the inner of polymeric micelles, the fluorescence of star-conjugated polymer and drug was quenched. The fluorescence change of DOX-loaded polymeric micelles showed good correlation with the drug release at different time intervals. The real-time release of drug as well as the fluorescence signals was monitored directly by fluorescence microscope. Owing to the high efficiency of cellular uptake and subsequent acidic environment in tumor cells, DOX-loaded HCP-N-PEG micelles showed the fast DOX release in the MCF-7 cells upon the cleavage of acylhydrazone bond. In contrast, the DOX-loaded HCP-O-PEG micelles had lower release rate of DOX. This different release rate of DOX could lead to discriminable cytotoxicity of DOX-loaded polymeric micelles to the tumor cells. Such a self-assembled star-conjugated copolymer with high fluorescence exploits its new platform in polymeric drug delivery systems.

#### ■ ASSOCIATED CONTENT

##### Supporting Information

Characterization of degree of branching of HCP-CHO; grafting ratio of HCP-N-PEG and HCP-O-PEG; GPC and TGA data of HCP-CHO and HCP-N-PEG and HCP-O-PEG; dimensions and morphologies of HCP-O-PEG and HCP-N-PEG micelles; cellular internalization of DOX-loaded HCP-O-PEG and HCP-N-PEG micelles. This material is available free of charge via the Internet at <http://pubs.acs.org>.

#### ■ AUTHOR INFORMATION

##### Corresponding Authors

\*E-mail: xyzhu@sjtu.edu.cn. Tel.: +86-21-34203400. Fax: +86-21-54741297.

\*E-mail: luucla@ucla.edu

\*E-mail: firstzq@sjtu.edu.cn

##### Notes

The authors declare no competing financial interest.

#### ■ ACKNOWLEDGMENTS

This work is sponsored by National Basic Research Program (2012CB821500, 2013CB834506), the Open Project of State Key Laboratory of Chemical Engineering (SKL-ChE-12C04), and China National Funds for Distinguished Young Scientists (21025417). The authors thank Mr. Hongying Chen for taking the bioexperiments.

#### ■ REFERENCES

- (1) Jeong, B.; Bae, Y. H.; Lee, D. S.; Kim, S. W. *Nature* **1997**, *388*, 860–862.
- (2) Uhrich, K. E.; Cannizzaro, S. M.; Langer, R. S.; Shakesheff, K. M. *Chem. Rev.* **1999**, *99*, 3181–3198.
- (3) Duncan, R. *Nat. Rev. Drug Discovery* **2003**, *2*, 347–360.
- (4) Knop, K.; Hoogenboom, R.; Fischer, D.; Schubert, U. S. *Angew. Chem., Int. Ed.* **2010**, *49*, 6288–6308.
- (5) Zhang, L.; Gu, F. X.; Chan, J. M.; Wang, A. Z.; Langer, R. S.; Farokhzad, O. C. *Clin. Pharmacol. Ther.* **2008**, *83*, 761–769.
- (6) Zhang, L. F.; Chan, J. M.; Gu, F. X.; Rhee, J. W.; Wang, A. Z.; Radovic-Moreno, A. F.; Alexis, F.; Langer, R.; Farokhzad, O. C. *ACS Nano* **2008**, *2*, 1696–1702.
- (7) Li, G. L.; Liu, J. Y.; Pang, Y.; Wang, R. B.; Mao, L. M.; Yan, D. Y.; Zhu, X. Y.; Sun, J. *Biomacromolecules* **2011**, *12*, 2016–2026.
- (8) Zhou, Y. F.; Huang, W.; Liu, J. Y.; Zhu, X. Y.; Yan, D. Y. *Adv. Mater.* **2010**, *22*, 4567–4590.
- (9) Langer, R. *Nature* **1998**, *392*, 5–10.

- (10) Davis, M. E.; Chen, Z.; Shin, D. M. *Nat. Rev. Drug Discovery* **2008**, *7*, 771–782.
- (11) Zhu, H. G.; McShane, M. J. *J. Am. Chem. Soc.* **2005**, *127*, 13448–13449.
- (12) Jana, A.; Devi, K. S. P.; Maiti, T. K.; Singh, N. D. P. *J. Am. Chem. Soc.* **2012**, *134*, 7656–7659.
- (13) Wang, J.; Wang, Y. G.; Liang, W. *J. Controlled Release* **2012**, *160*, 637–651.
- (14) Yang, X. Q.; Grailer, J. J.; Rowland, I. J.; Javadi, A.; Hurley, S. A.; Matson, V. Z.; Steeber, D. A.; Gong, S. Q. *ACS Nano* **2010**, *4*, 6805–6817.
- (15) Terry, C. M.; Li, L.; Li, H.; Zhuplatov, I.; Blumenthal, D. K.; Kim, S. E.; Owen, S. C.; Kholmovski, E. G.; Fowers, K. D.; Rathi, R.; Cheung, A. K. *J. Controlled Release* **2012**, *160*, 459–467.
- (16) Deckers, R.; Moonen, C. T. W. *J. Controlled Release* **2010**, *148*, 25–33.
- (17) Wadhwa, R.; Lagenaur, C. F.; Cui, X. T. *J. Controlled Release* **2006**, *110*, 531–541.
- (18) Mora, L.; Chumbimuni-Torres, K. Y.; Clawson, C.; Hernandez, L.; Zhang, L. F.; Wang, J. *J. Controlled Release* **2009**, *140*, 69–73.
- (19) Zhu, Q.; Qiu, F.; Zhu, B. S.; Zhu, X. Y. *RSC Adv.* **2013**, *3*, 2071–2083.
- (20) Zhang, J.; Campbell, R. E.; Ting, A. Y.; Tsien, R. Y. *Nat. Rev. Mol. Cell Biol.* **2002**, *3*, 906–918.
- (21) Medintz, I. L.; Uyeda, H. T.; Goldman, E. R.; Mattoussi, H. *Nat. Mater.* **2005**, *4*, 435–446.
- (22) Yang, J.; Zhang, Y.; Gautam, S.; Liu, L.; Dey, J.; Chen, W.; Mason, R. P.; Serrano, C. A.; Schug, K. A.; Tang, L. *Proc. Natl. Acad. Sci. U.S.A.* **2009**, *106*, 10086–10091.
- (23) Wu, C. F.; Szymanski, C.; Cain, Z.; McNeill, J. *J. Am. Chem. Soc.* **2007**, *129*, 12904–12905.
- (24) Sigurdson, C. J.; Peter, K.; Nilsson, R.; Hornemann, S.; Mancio, G.; Polymenidou, M.; Schwarz, P.; Leclerc, M.; Hammarstrom, P.; Wuthrich, K.; Aguzzi, A. *Nat. Methods* **2007**, *4*, 1023–1030.
- (25) Tang, H. W.; Xing, C. F.; Liu, L. B.; Yang, Q.; Wang, S. *Small* **2011**, *7*, 1464–1470.
- (26) Thomas, S. W.; Joly, G. D.; Swager, T. M. *Chem. Rev.* **2007**, *107*, 1339–1386.
- (27) Yin, M.; Shen, J.; Pflugfelder, G. O.; Mullen, K. *J. Am. Chem. Soc.* **2008**, *130*, 7806–7807.
- (28) Qiu, F.; Tu, C. L.; Wang, R. B.; Zhu, L. J.; Chen, Y.; Tong, G. S.; Zhu, B. S.; He, L.; Yan, D. Y.; Zhu, X. Y. *Chem. Commun.* **2011**, *47*, 9678–9680.
- (29) Qiu, F.; Wang, D. L.; Wang, R. B.; Huan, X. Y.; Tong, G. S.; Zhu, Q.; Yan, D. Y.; Zhu, X. Y. *Biomacromolecules* **2013**, *14*, 1678–1686.
- (30) Qiu, F.; Tu, C. L.; Chen, Y.; Shi, Y. F.; Song, L.; Wang, R. B.; Zhu, X. Y.; Zhu, B. S.; Yan, D. Y.; Han, T. *Chem.—Eur. J.* **2010**, *16*, 12710–12717.
- (31) Hamal, S.; Hirayama, F. *J. Phys. Chem.* **1983**, *87*, 83–89.
- (32) Zhu, L. J.; Shi, Y. F.; Tu, C. L.; Wang, R. B.; Pang, Y.; Qiu, F.; Zhu, X. Y.; Yan, D. Y.; He, L.; Jin, C. Y.; Zhu, B. S. *Langmuir* **2010**, *26*, 8875–8881.
- (33) Zhou, Y. F.; Yan, D. Y. *Chem. Commun.* **2009**, *45*, 1172–1188.
- (34) Wang, D. L.; Chen, H. Y.; Su, Y.; Qiu, F.; Zhu, L. J.; Huan, X. Y.; Zhu, B. S.; Yan, D. Y.; Guo, F. L.; Zhu, X. Y. *Polym. Chem.* **2013**, *4*, 85–94.
- (35) Feng, X. L.; Lv, F. T.; Liu, L. B.; Tang, H. W.; Xing, C. F.; Yang, Q. O.; Wang, S. *ACS Appl. Mater. Interfaces* **2010**, *2*, 2429–2435.
- (36) Lv, W.; Li, N.; Li, Y. L.; Li, Y.; Xia, A. D. *J. Am. Chem. Soc.* **2006**, *128*, 10281–10287.
- (37) Wang, F.; Wang, Y. C.; Dou, S.; Xiong, M. H.; Sun, T. M.; Wang, J. *ACS Nano* **2011**, *5*, 3679–3692.
- (38) Zhu, L. J.; Tu, C. L.; Zhu, B. S.; Su, Y.; Pang, Y.; Yan, D. Y.; Wu, J. L.; Zhu, X. Y. *Polym. Chem.* **2011**, *2*, 1761–1768.
- (39) Ke, C. J.; Chiang, W. L.; Liao, Z. X.; Chen, H. L.; Lai, P. S.; Sun, J. S.; Sung, H. W. *Biomaterials* **2013**, *34*, 1–10.
- (40) Santra, S.; Kaittanis, C.; Santiesteban, O. J.; Perez, J. M. *J. Am. Chem. Soc.* **2011**, *133*, 16680–16688.
- (41) Jana, A.; Devi, K. S. P.; Maiti, T. K.; Singh, N. D. P. *J. Am. Chem. Soc.* **2012**, *134*, 7656–7659.
- (42) Lai, J. P.; Shah, B. P.; Garfunkel, E.; Lee, K. B. *ACS Nano* **2013**, *7*, 2741–2750.
- (43) Weinstain, R.; Segal, E.; Satchi-Fainaro, R.; Shabat, D. *Chem. Commun.* **2010**, *46*, 553–555.
- (44) Wang, D. L.; Su, Y.; Jin, C. Y.; Zhu, B. S.; Pang, Y.; Zhu, L. J.; Liu, J. Y.; Tu, C. L.; Yan, D. Y.; Zhu, X. Y. *Biomacromolecules* **2011**, *12*, 1370–1379.
- (45) Zhang, W. L.; Li, Y. L.; Liu, L. X.; Sun, Q. Q.; Shuai, X. T.; Zhu, W.; Chen, Y. M. *Biomacromolecules* **2010**, *11*, 1331–1338.